

# Thermal Stability and Emissivity Behavior (7-14 $\mu\text{m}$ ) of Ca-Sulfides under Simulated Daytime Surface Conditions for Multiple Mercury days: Implications for the formation of hollows and CaS detection by MERTIS onboard the 3 BepiColombo mission

Indhu Varatharajan<sup>1</sup>, Claudia Stangarone<sup>1</sup>, Sergio Speziale<sup>2</sup>, Alessandro Maturilli<sup>3</sup>, Jörn Helbert<sup>1</sup>, Harald Hiesinger<sup>4</sup>, Iris Weber<sup>4</sup>, and Karin E Bauch<sup>4</sup>

<sup>1</sup>Institute of Planetary Research, German Aerospace Center (DLR), Berlin, Germany

<sup>2</sup>Helmholtz Centre Potsdam -GFZ German Research Centre for Geosciences

<sup>3</sup>Institute of Planetary Research, German Aerospace Center (DLR), Berlin, Germany.

<sup>4</sup>Westfälische Wilhelms-Universität Münster

November 26, 2022

## Abstract

Global mapping of the nature and distribution of volatiles such as sulfides on Mercury's surface is essential for understanding the thermal evolution of the planet. The surface exposure of these sulfides over extreme day-night temperature cycles (176 days; 450 degC to -170 degC) on Mercury leads to thermal weathering of these sulfide compounds. It has been seen that among the proposed sulfides on Mercury (MgS, FeS, CaS, CrS, TiS, NaS, and MnS), CaS showed relatively stable and distinctive spectral features in the thermal infrared region (TIR; 7-14  $\mu\text{m}$ ) when studied under the simulated Mercury day conditions for temperatures ranging from 100 degC up to 500 degC under vacuum (0.1 mbar) (Varatharajan et al., 2019). In this study, we re-investigated the stability of CaS and its spectral emissivity spectral behavior. We exposed the sample for four consecutive Earth days simulating Mercury day cycles and measured the TIR spectra of CaS for temperatures up to 500 degC (with steps of 100 degC) every day. This time the spectral analysis is coupled and supported by XRD diffraction on the fresh and temperature-processed sample, showing the mineralogical evolution with temperature. We confirm that CaS is a stable compound and therefore it would remain stable on Mercury's surface regardless of investigated peak surface temperatures. This study further implies that, for the hollows dominated by the sublimation of sulfides on Mercury (Blewett et al., 2013; Helbert et al., 2013a; Vilas et al., 2016), CaS could be the last of the sulfides that could be mapped on Mercury as other sulfides were lost by thermal decomposition, leaving behind hollows. This could make CaS an important tracer for other sulfides, which might be lost in the hollow-forming process and supports the detection of CaS within hollows by MESSENGER (Vilas et al., 2016). The emissivity spectra reported here are significant for the detection and mapping of CaS associated with hollows and pyroclastics using the Mercury Radiometer and Thermal Imaging Spectrometer (MERTIS) datasets.

1 **Thermal Stability and Emissivity Behavior (7-14  $\mu\text{m}$ ) of Ca-Sulfides under**  
2 **Simulated Daytime Surface Conditions for Multiple Mercury days: Implications**  
3 **for the formation of hollows and CaS detection by MERTIS onboard the**  
4 **BepiColombo mission**

5 Indhu Varatharajan<sup>1,2</sup>, Claudia Stangarone<sup>1</sup>, Sergio Speziale<sup>3</sup>, Alessandro Maturilli<sup>1</sup>,  
6 Jörn Helbert<sup>1</sup>, Harald Hiesinger<sup>4</sup>, Iris Weber<sup>4</sup>, Karin E. Bauch<sup>4</sup>

7

8 <sup>1</sup>Department of Planetary Laboratories, Institute of Planetary Research, German  
9 Aerospace Center (DLR), Berlin, Germany.

10 <sup>2</sup>Institute of Geological Sciences, Freie University (FU) Berlin, Germany.

11 <sup>3</sup>Helmholtz Centre Potsdam - GFZ German Research Centre for Geosciences, Potsdam,  
12 Germany.

13 <sup>4</sup>Institut für Planetologie, Westfälische Wilhelms-Universität Münster, Germany

14

15

16

### **Highlights**

17 1. Spectral emissivity behavior (7-14  $\mu\text{m}$ ) of calcium-sulfides (CaS) remains  
18 stable for repeated heating cycles under simulated Mercury daytime surface  
19 conditions.

20 2. CaS is the stable sulfide that survives the extreme thermal environment of  
21 Mercury.

22 3. CaS is an important tracer for other sulfides those might be lost in the hollow-  
23 forming process dominated by sublimation.

24

25

26 **Abstract**

27 Global mapping of the nature and distribution of volatiles such as sulfides on  
28 Mercury's surface is essential for understanding the thermal evolution of the planet.  
29 The surface exposure of these sulfides over extreme day-night temperature cycles (176  
30 days; 450 °C to -170 °C) on Mercury leads to thermal weathering of these sulfide  
31 compounds. It has been seen that among the proposed sulfides on Mercury (MgS, FeS,  
32 CaS, CrS, TiS, NaS, and MnS), CaS showed relatively stable and distinctive spectral  
33 features in the thermal infrared region (TIR; 7-14 μm) when studied under the  
34 simulated Mercury day conditions for temperatures ranging from 100 °C up to 500 °C  
35 under vacuum (0.1 mbar) (Varatharajan et al., 2019). In this study, we re-investigated  
36 the stability of CaS and its spectral emissivity spectral behavior. We exposed the sample  
37 for four consecutive Earth days simulating Mercury day cycles and measured the TIR  
38 spectra of CaS for temperatures up to 500 °C (with steps of 100 °C) every day. This  
39 time the spectral analysis is coupled and supported by XRD diffraction on the fresh and  
40 temperature-processed sample, showing the mineralogical evolution with temperature.  
41 We confirm that CaS is a stable compound and therefore it would remain stable on  
42 Mercury's surface regardless of investigated peak surface temperatures. This study  
43 further implies that, for the hollows dominated by the sublimation of sulfides on  
44 Mercury (Blewett et al., 2013; Helbert et al., 2013a; Vilas et al., 2016), CaS could be  
45 the last of the sulfides that could be mapped on Mercury as other sulfides were lost by  
46 thermal decomposition, leaving behind hollows. This could make CaS an important  
47 tracer for other sulfides, which might be lost in the hollow-forming process and  
48 supports the detection of CaS within hollows by MESSENGER (Vilas et al., 2016). The  
49 emissivity spectra reported here are significant for the detection and mapping of CaS

50 associated with hollows and pyroclastics using the Mercury Radiometer and Thermal  
51 Imaging Spectrometer (MERTIS) datasets.

52 **Keywords:** Mercury; Thermal Weathering; Emissivity; Spectroscopy; CaS; Hollows

53

## 54 **1 Introduction**

55 NASA's MESSENGER (Mercury Surface, Space Environment, Geochemistry,  
56 and Ranging) mission revealed that Mercury, unlike the Moon, has been formed in a  
57 highly reducing environment with sulfur abundances of up to 4 wt% (Nittler et al.,  
58 2011). MESSENGER's XRS (X-Ray Spectrometer) data suggest that FeS and CaS are  
59 present in Mercury's shallow regolith, with minor MnS and NaCrS<sub>2</sub> (Nittler et al., 2011;  
60 Weider et al., 2016). Thermochemical and experimental evidence indicates that CaS is  
61 the major lithophile sulfide on Mercury (Vaughan, 2013), supported by MESSENGER  
62 XRS data, which showed a strong correlation in the detected abundances of Ca and S,  
63 suggesting the presence of minerals such as oldhamites (Nittler et al., 2011; Weider et  
64 al., 2016; Weider et al., 2014; Weider et al., 2012). Sulfides have been proposed to be  
65 present at unique sub-km scale landforms called hollows (Helbert et al., 2013a). This  
66 hypothesis has been supported by the first spectral evidence of sulfide minerals (CaS,  
67 MgS) within the hollows of Dominici crater detected by MESSENGER Mercury Dual-  
68 Imaging System (MDIS) that mapped Mercury's surface in the visible-infrared spectral  
69 region (400 to 1000 nm) (Vilas et al., 2016). The global spectral mapping of identified  
70 hollows and pyroclastics utilizing at wide spectral ranges will enable us to effectively  
71 map the sulfide materials across Mercury's surface (Besse et al., 2020; Helbert et al.,  
72 2013a; Lucchetti et al., 2018; Thomas et al., 2014a, b; Vilas et al., 2016).

73 The Mercury Radiometer and Thermal Imaging Spectrometer (MERTIS)  
74 onboard the Mercury Planetary Orbiter (MPO) of ESA/JAXA's BepiColombo mission

75 will be the first orbital thermal infrared spectrometer (TIS) and radiometer (TIR) to map  
76 the surface mineralogy in the mid-infrared spectral range (Hiesinger et al., 2020;  
77 Hiesinger et al., 2010). With its two channels (TIS, TIR), MERTIS will characterize  
78 the emissivity behavior of surface materials, including sulfides, between 7  $\mu\text{m}$  and 14  
79  $\mu\text{m}$  (TIS) (between 7  $\mu\text{m}$  and 40  $\mu\text{m}$  with TIR) with a spectral resolution of 90 nm (78  
80 spectral channels) and a spatial resolution of 500m/pixel along with its corresponding  
81 surface temperature.

82 In a recent study (Varatharajan et al., 2019), the emissivity behavior of a wide  
83 range of sulfides (MgS, FeS, CaS, CrS, TiS, NaS, and MnS) within the MERTIS  
84 spectral range (7-14 $\mu\text{m}$ ) were studied for temperatures ranging from 100  $^{\circ}\text{C}$  up to 500  
85  $^{\circ}\text{C}$ , with heating steps of 100  $^{\circ}\text{C}$  under vacuum (0.1 mbar). The study showed that,  
86 among these sulfides, only CaS exhibited strong emissivity features and minor  
87 susceptibility to thermal weathering while reaching extreme temperatures of 500  $^{\circ}\text{C}$  for  
88 one simulated Mercury day (Varatharajan et al., 2019).

89 Mercury's surface is repeatedly exposed to extreme temperature changes,  
90 ranging from 450  $^{\circ}\text{C}$  during daytime to -170  $^{\circ}\text{C}$  during nighttime over a one day/night  
91 cycle of 176 terrestrial days (Krotikov and Shchuko, 1975; Soter and Ulrichs, 1967). In  
92 this study, we aim at further investigating the physical/thermal and emissivity/spectral  
93 stability of CaS while exposed to an extreme thermal environment for multiple  
94 simulated Mercury days as a function of temperature (100  $^{\circ}\text{C}$ , 200  $^{\circ}\text{C}$ , 300  $^{\circ}\text{C}$ , 400  $^{\circ}\text{C}$ ,  
95 and 500  $^{\circ}\text{C}$ ) under vacuum (0.1 mbar) for each day (see Section 2.1). For the whole  
96 duration of the experiment, the vacuum was maintained inside the emissivity chamber.  
97 The physical stability of CaS is studied by X-Ray diffraction (XRD) analysis of the  
98 starting (fresh synthetic) CaS and the resulting thermally processed CaS after four  
99 simulated Mercury days (Section 2.2). Our study is important for understanding the

100 thermal stability of the volatile-bearing materials such as CaS under Mercury daytime  
101 surface conditions for their effective detection from the orbit by MERTIS.

102

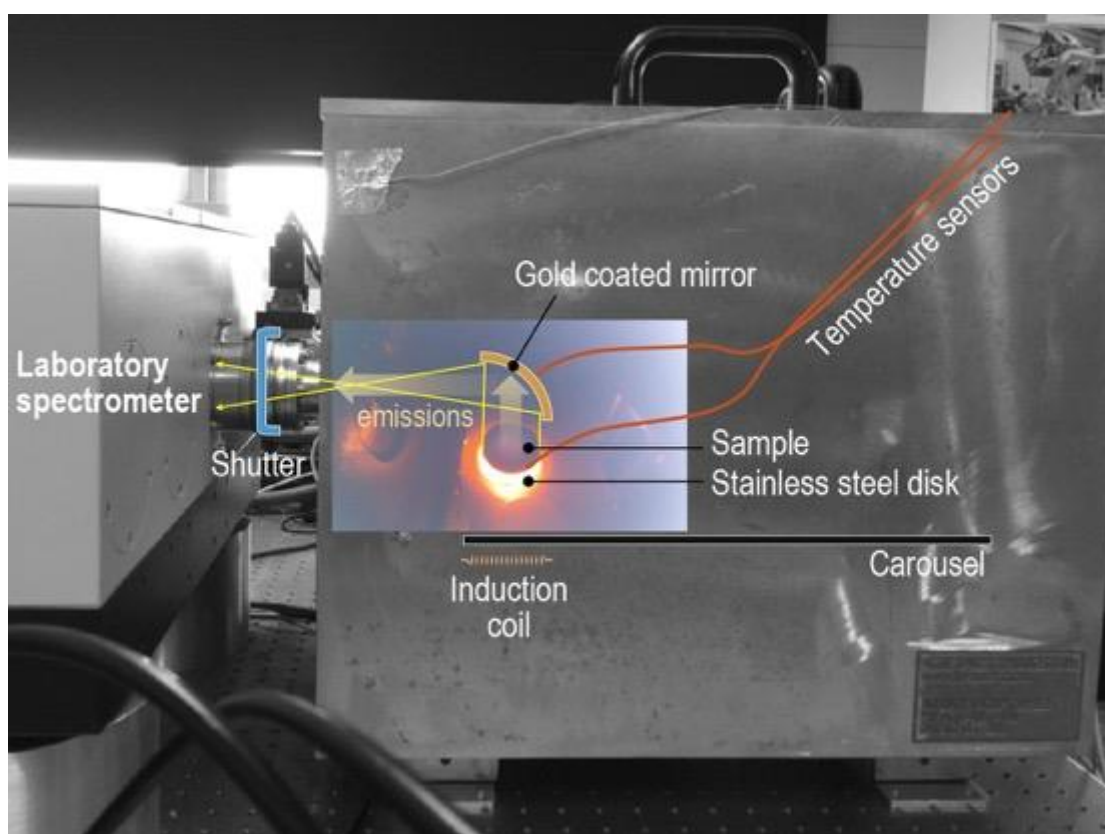
## 103 **2. Sample, Facility and Methods**

104 For this study, the starting material used is synthetic CaS with a grain size of  
105 ~10  $\mu\text{m}$  (certified by industrial supplier Alfa Aesar; CAS No. 20548-54-3) as used in  
106 the study by (Varatharajan et al., 2019). The facility and methods for emissivity and x-  
107 ray diffraction studies are explained below in sections 2.1 and 2.2 respectively.

### 108 **2.1 Emissivity**

109 Planetary Spectroscopy Laboratory (PSL) is located at the Institute of Planetary  
110 Research, German Aerospace Center (DLR) in Berlin, Germany. Among the facilities  
111 present at PSL, the emissivity chamber allows to heat up various analogue materials,  
112 reaching extreme temperatures and to study their emissivity behaviors as a function of  
113 temperature (50  $^{\circ}\text{C}$ -600  $^{\circ}\text{C}$ ) across a wide spectral range (1-50  $\mu\text{m}$ ). The systematic  
114 emissivity studies results in an extensive planetary materials emissivity library. Such  
115 specialized spectral library is created to support surface composition analyses of hot  
116 planetary targets such as Mercury, Venus, Moon, and Io (Helbert et al., 2019; Helbert  
117 and Maturilli, 2009; Helbert et al., 2013a; Helbert et al., 2013b; Maturilli et al., 2008;  
118 Varatharajan et al., 2019). One of the three identical FTIR (Fourier transform infrared)  
119 spectrometers (Bruker Vertex 80V) at PSL is connected to the external emissivity  
120 chamber (Fig. 1). The spectrometer is optimized for spectral measurements under  
121 vacuum conditions (0.1 mbar). The chamber is separated from the spectrometer by a  
122 shutter and a vacuum-tight optical window between the chamber and the spectrometer,  
123 enabling the chamber to be operated under vacuum or at the desired pressure condition.

124 For this study, the fresh CaS sample is placed in a stainless-steel cup which is  
125 then placed on a carousel, that can be rotated via a stepper motor to bring several  
126 samples to the measurement position without breaking the vacuum inside the chamber.  
127 The sample is heated from below the carousel (made of quartz glass) by an induction  
128 system. The temperature of the sample cup is controlled by adjusting the current applied  
129 to the induction coil. Three temperature sensors (thermopiles) on the sample and on the  
130 side of the sample cup, continuously monitor the bulk surface temperature, while the  
131 surrounding environment of the sample is monitored by a webcam (Fig. 1). The  
132 spectrometer is equipped with MCT HgCdTe detector (cooled by liquid nitrogen) and  
133 KBr beamsplitter to study the emissivity behavior of CaS at the TIR spectral region (7-  
134 14  $\mu\text{m}$ ) at the spectral resolution of  $4\text{ cm}^{-1}$  under vacuum.

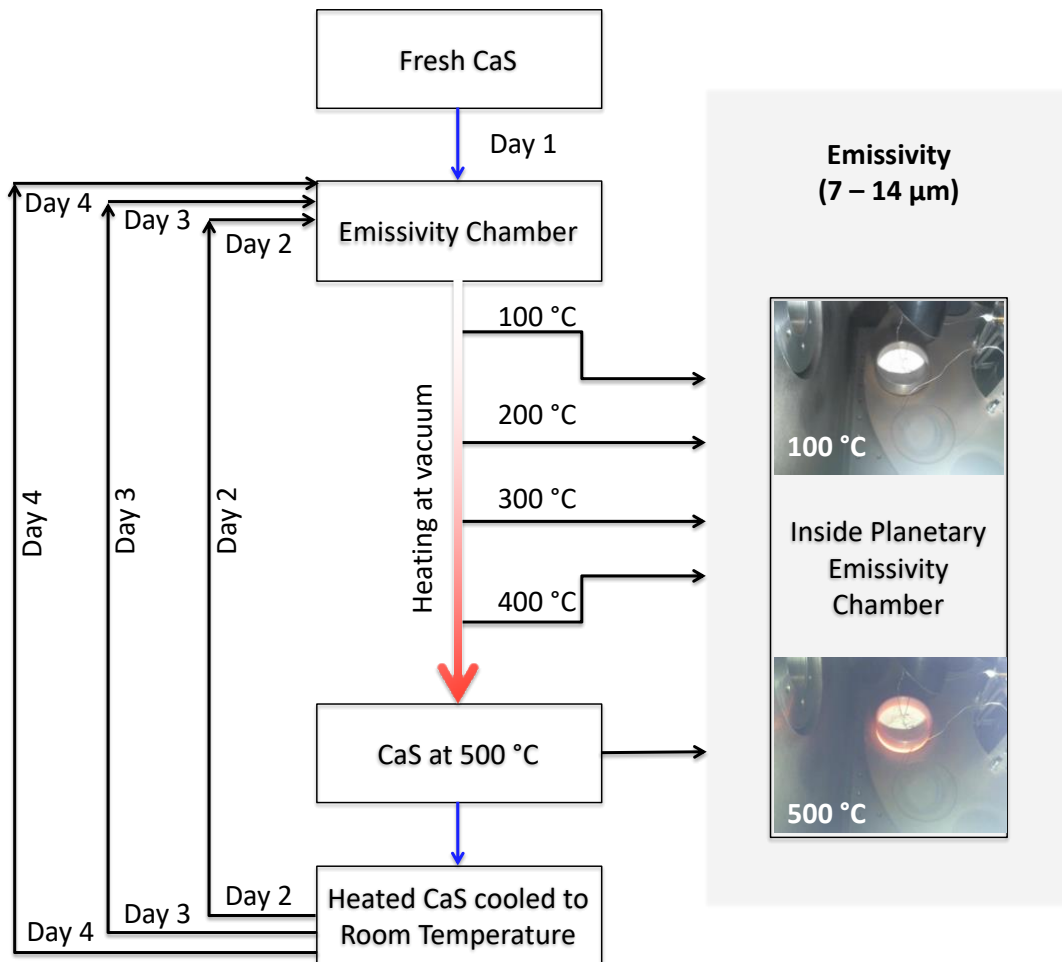


135  
136 **Figure 1.** Graphical illustration of the laboratory set-up at PSL for high temperature  
137 emissivity measurements. The figure shows the heating of the sample cup using  
138 induction coil and its corresponding emissions been deflected to the Bruker 80V  
139 spectrometer using a gold-coated mirror. The image from inside the chamber was taken  
140 by a webcam during the measurement. The samples are placed in a stainless-steel disk,

141 which is then placed on the carousel. The induction coil heats the sample cup through  
142 the carousel. The shutter between the spectrometer and the emissivity chamber enables  
143 us to physically detach the emissivity chamber and spectrometer while heating under  
144 vacuum and therefore protecting the spectrometer from continuous heat emissions. The  
145 shutter is open only while recording the measurements when sample cup reaches its  
146 desired temperatures.  
147

148 In this study, the emissivity spectral measurements of CaS are conducted for  
149 four simulated Mercury days each. The simple graphical flowchart of the experimental  
150 procedure is shown in Fig. 2. The detailed step by step experimental procedure is  
151 explained below:

152



153  
154  
155  
156  
157  
158  
159

**Figure 2.** Graphical summary of the methodology used in the study to measure the emissivity of calcium sulfides (CaS) for four heating cycles during which the sample surface temperatures reach up to 500°C. The experimental set-up inside the emissivity chamber is also shown for temperatures 100 °C and 500 °C.

160           1. Once the experimental setup is ready and the fresh CaS sample loaded, both  
161 the spectrometer and the chamber are slowly evacuated. Before heating up, the sample  
162 is kept under vacuum for at least 1 hour to purge it from any air trapped in the sample.  
163 In the meantime, the detector is cooled down by liquid nitrogen.

164           2. Once the instrument and the chamber are stabilized under vacuum conditions,  
165 CaS is slowly heated up by manually controlling the current to the induction system.  
166 When the sample surface is stable at 100 °C, the first measurement takes place. The  
167 shutter between the chamber and the spectrometer opens, allowing the spectrometer to  
168 detect the radiance coming from the heated surface of CaS. The radiance is collected  
169 and deflected by a gold (Au) coated parabolic mirror at 90° off-axis into the  
170 spectrometer. After the measurement, the shutter is closed again to avoid that any  
171 particle reaches the spectrometer optics during heating process.

172           3. This procedure is repeated at temperatures of 200 °C, 300 °C, 400 °C, and  
173 500 °C, thus obtaining the emissivity measurements for 1<sup>st</sup> simulated Mercury day.

174           4. After the last measurement at 500 °C, the chamber and the thermally  
175 processed CaS sample cool down overnight reaching room temperature. The vacuum  
176 condition is kept constant during the entire process. During the entire heating period,  
177 the CaS sample cup is never moved and is carefully monitored with the webcam  
178 installed in the chamber to detect outgassing events.

179           5. Each step from 2 to 4 is repeated every day for another three consecutive  
180 Earth days simulating a Mercury day cycle where the surface reaches up to 500 °C. For  
181 all the four days of measurements, the vacuum pump is continuously operated. The  
182 samples are therefore not exposed to the atmosphere during the entire experiment (Fig.  
183 2).

184           At the end of the measurements, the CaS sample used for the measurements is  
185 by all means thermally processed (T-processed) under Mercury daytime temperatures.  
186 All the measured emissivity spectra of CaS, which are shown in Figure 3, are finally  
187 calibrated against a blackbody reference at their respective measured temperatures and  
188 geometric configurations. PSL uses blast furnace slag as a standard blackbody for the  
189 temperatures and spectral range used in this study (Maturilli et al., 2013).

190

## 191 **2.2 X-Ray Diffraction (XRD)**

192           In order to understand the physical stability of CaS under the extreme thermal  
193 environment of Mercury and to explain the observed changes in its spectral  
194 characteristics (Fig. 3), the XRD analyses of the fresh starting material (CaS) and the  
195 recovered thermally processed CaS were conducted at the Helmholtz Centre Potsdam -  
196 GFZ German Research Centre for Geosciences, Potsdam. The instrument used for the  
197 XRD analyses is a STOE STADI P powder diffractometer. The primary Cu  $K_{\alpha 1}$   
198 radiation was produced with 40 kV acceleration voltage and 40 mA beam current and  
199 a Ge (111) primary monochromator. The diffracted radiation was detected by a high-  
200 resolution DECTRIS MYTHEN detector. Measurements were performed in the range  
201  $2\theta = 5^{\circ}$ - $100^{\circ}$  where  $2\theta$  is the angle between incident X-ray beam and reflected X-ray  
202 beam. The accuracy of the system was monitored before each measurement by  
203 collecting a full X-ray diffraction spectrum of Si standard (NIST 640d). The average  
204 value of the unit-cell parameter of Si is  $5.430 \pm 0.001 \text{ \AA}$ , which, compared to the  
205 certified value  $a_0 = 5.43123 \pm 0.00008 \text{ \AA}$ , corresponds to an accuracy of 0.02%.

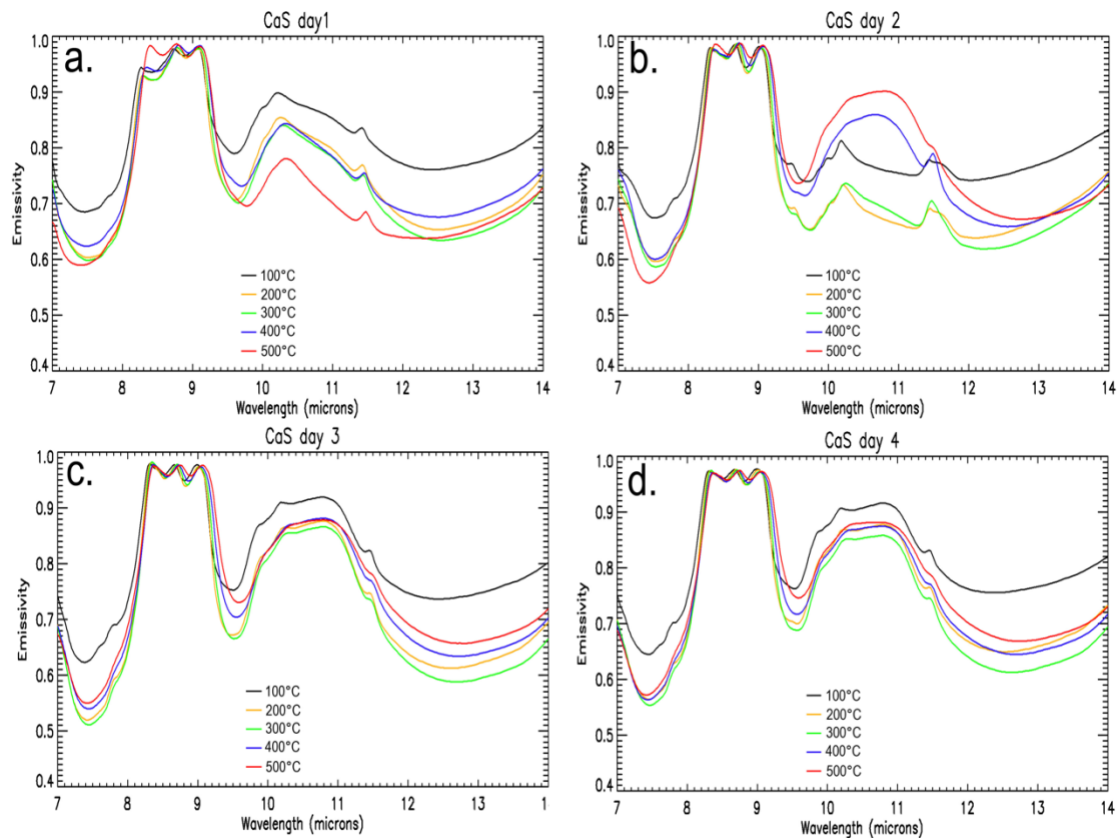
206           The results obtained from the XRD measurements for starting and thermally  
207 processed CaS are shown in Fig. 4a and Fig. 4b respectively and are discussed in detail  
208 in Section 3.2

209 **3. Results and Discussions**

210 **3.1 Emissivity measurements**

211 The spectral evolution of calibrated emissivity of the CaS for four simulated  
212 Mercury days is discussed below:

213



214  
215

216 **Figure 3.** (a-d) Emissivity measurements showing emissivity behavior of CaS under  
217 four simulated Mercury daytime surface conditions where peak surface temperatures  
218 reach upto 400-500°C. (b) The evolution of an emissivity feature near 10-11  $\mu\text{m}$  is  
219 observed for samples heated to  $>400^\circ\text{C}$  during second simulated Mercury day. (c-d)  
220 However, the spectra remained constant during the third and fourth day.

221  
222  
223

224 *Simulated Mercury Day 1:* With the increase of temperature from 100 to 500  
225  $^\circ\text{C}$  during the first simulated Mercury day (Fig. 3a). We observed that: a) The band  
226 center near 7.5  $\mu\text{m}$  remains constant until the sample reaches 400  $^\circ\text{C}$ , dropping  
227 shortwards to  $\sim 7.4 \mu\text{m}$  at 500  $^\circ\text{C}$ ; b) The emissivity shows a maximum doublet near 8.8  
228  $\mu\text{m}$  and this spectral feature does not change in strength and position when heating from

228 100 °C to 400 °C, whereas at 500 °C, the emissivity near the 8.3 μm spectral shoulder  
229 slightly increases; c) The band center near 9.6 μm does not change until heating up to  
230 300 °C but slightly shifts to longer wavelengths with increasing temperatures from 300  
231 °C to 500 °C; d) The center of the spectral shoulder near 10.2 μm and the spectral spike  
232 near 11.4 μm slightly increase with increasing temperatures from 100 °C to 500 °C; and  
233 e) The emissivity for spectral features near 7.5 μm and 9.5 μm decreases with increasing  
234 temperatures.

235 ***Simulated Mercury Day 2:*** Emissivity spectra of CaS at 100 °C (Fig. 3b; black)  
236 during Day 2 show comparatively similar spectral shapes compared to emissivity  
237 spectra of CaS at 500 °C of Day 1 (Fig. 3a; red). Within the spectral region of 7.5-9.5  
238 μm, the overall spectral morphology remains stable while heating up to 500 °C.  
239 However, the spectral shape at wavelength larger than 12 μm changes drastically when  
240 the sample temperature exceeds 400 °C. Up to 300 °C, the spectral shape between 10  
241 μm and 12 μm display a negative slope having spectral shoulders (minor peaks in  
242 emissivity) at 10.2 μm and 11.4 μm. However, at temperatures 400 °C, this spectral  
243 slope evolves into a broad emissivity band. This spectral feature is also observed in  
244 spectra taken at 500 °C with a slight increase in emissivity.

245 ***Simulated Mercury Day 3:*** In order to test the stability of the emissivity spectra  
246 of CaS at the end of the measurements at Day 2 (Fig.3b; red), the emissivity procedure  
247 is repeated again for Day 3. At temperature of 100 °C (Fig. 3c; black) during Day 3, the  
248 emissivity of CaS maintains the spectral shape of CaS at 400 °C and 500 °C during the  
249 previous day (Fig. 3b; red). While heating through 200°, 300°, 400°, and 500°C, the  
250 general spectral morphology of the emissivity behavior of CaS did not show any  
251 significant changes. For all temperatures, a) the emissivity of CaS during Day 3 shows  
252 minima at ~7.5 μm and 9.5 μm, b) the emissivity maximum shows a doublet feature

253 centered around  $\sim 8.8 \mu\text{m}$ , and c) the spectral shape between 10 and 12  $\mu\text{m}$  feature shows  
254 a broad spectral band in contrast to the spectral shape of Day 1.

255 ***Simulated Mercury Day 4:*** When the sample was heated again through the  
256 fourth simulated Mercury day (100-500 °C) under vacuum, the emissivity spectra  
257 remained unchanged with respect to the previous day (Day 3) at all respective  
258 temperatures.

259 At the end of the four days of emissivity measurements of the CaS sample under  
260 vacuum, a mild “rotten egg” odor was sensed while opening the chamber. This may  
261 indicate the release of S during the experiments.

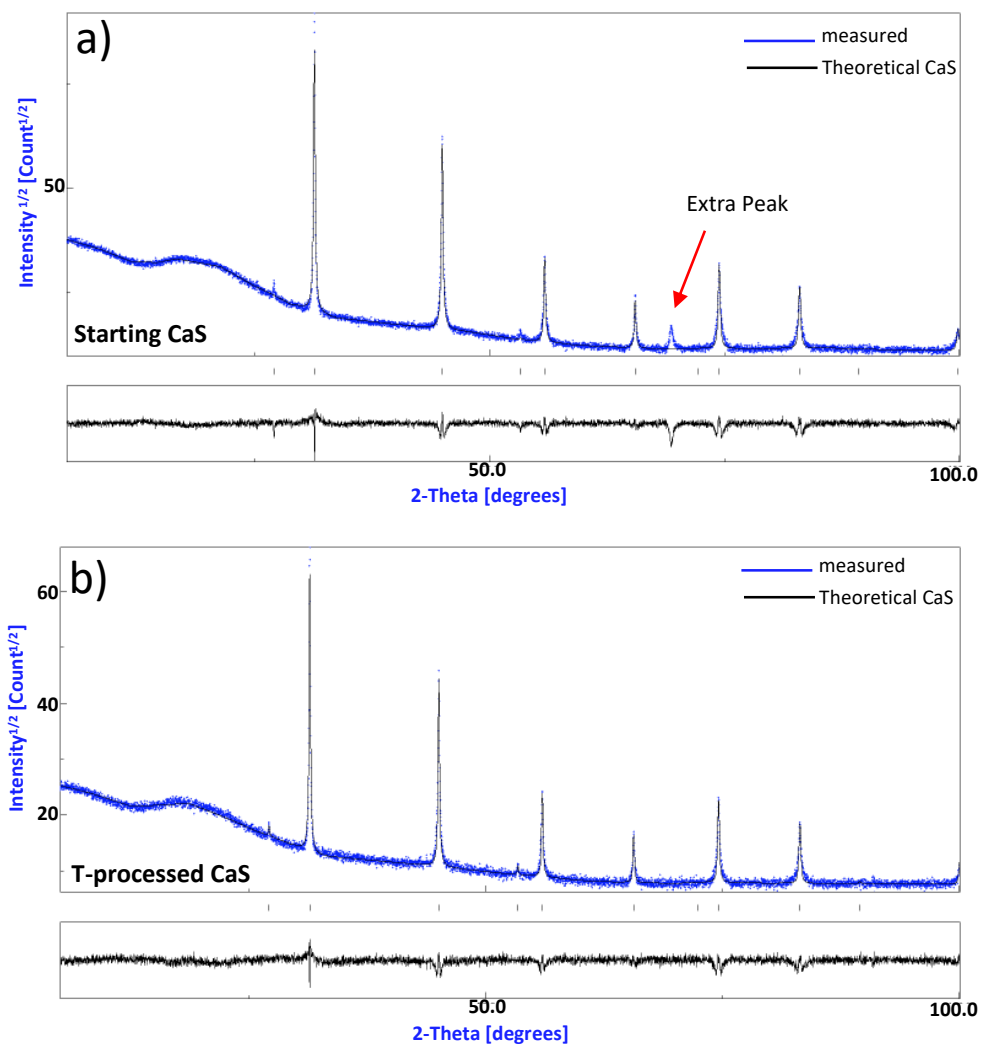
### 262 **3.2 XRD Analysis**

263 In order to explain the changes in spectral characteristics of fresh CaS and the  
264 products after four heating cycles (Fig. 3), XRD analyses were conducted for the fresh  
265 starting CaS (corresponding to emissivity spectra during Day 1) and the resulting  
266 thermally processed CaS (corresponding to emissivity spectra during Day 4).

267 The measured XRD diffractogram of the starting/fresh CaS against the  
268 theoretical XRD diffractogram of pure CaS is plotted in Fig. 4a. The measured XRD  
269 diffractogram of our fresh CaS displays an extra peak (d-spacing at circa 1.35 Å)  
270 marked as red arrow in Fig. 4a which does not belong to the calculated XRD pattern of  
271 pure CaS. This extra peak is probably due to minor impurities in the starting material  
272 of the synthetic CaS sample. Hence, the emissivity spectra of CaS at all temperatures  
273 for Day 1 (Fig. 3a) does not correspond to the emissivity spectra of pure CaS.

274 However, this extra peak (d-spacing at circa 1.35 Angstrom) disappeared in the  
275 measured XRD pattern of the thermally processed (T-processed) CaS, which matches  
276 with all the peaks attributed to the calculated XRD pattern of pure CaS as shown in Fig.  
277 4b. This disappearance of the extra peak in the T-processed CaS can be explained as,

278 impurities within the starting sample that either become amorphous or cryptocrystalline  
279 or even sublimated in the process of repeated heating up to 500 °C (Fig 4b). The match  
280 of the peaks of the measured XRD pattern of the thermally processed sample with the  
281 calculated XRD pattern of pure CaS (shown in Fig. 4b) confirms the thermal stability  
282 of CaS. Hence, the emissivity spectra of CaS at Day 4 at all temperatures correspond to  
283 the emissivity spectrum of pure CaS which is stable at even the extreme temperatures  
284 of Mercury and during repeated heating cycles.



285  
286  
287 **Figure 4.** The XRD diffratogram results obtained for (a) fresh CaS and (b) thermally  
288 processed CaS after four heating cycles. The top plot for both (a) and (b) compares the  
289 measured (blue-dotted) and calculated XRD pattern of CaS (black solid). The bottom  
290 plot for both (a) and (b) shows the difference between observed and calculated XRD  
291 amplitudes of CaS. The presence of impurities in the starting/fresh CaS sample is  
292 indicated by the extra peak (d-spacing at circa 1.35 Angstrom) in the measured XRD

293 pattern of the starting sample in (a) marked by red arrow. This extra peak (d-spacing at  
294 circa 1.35 Angstrom) disappeared in the measured XRD pattern of the thermally  
295 processed CaS in (b) which could suggest that these impurities get amorphous or  
296 cryptocrystalline or even sublimated after heating upto 500 °C.  
297

298

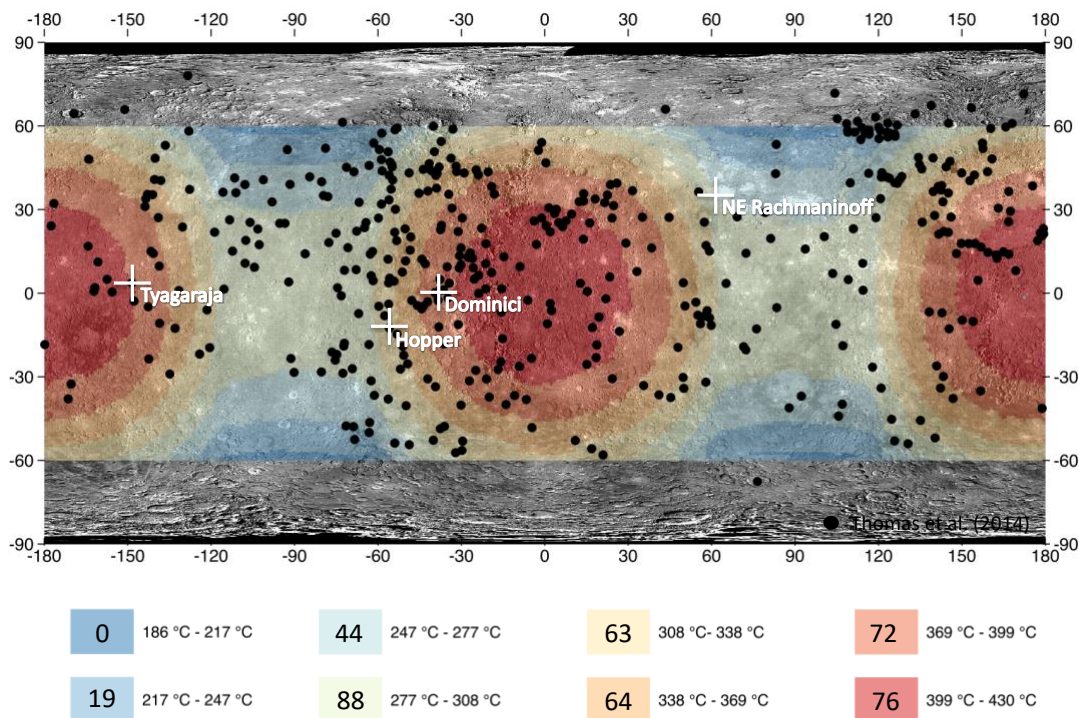
#### 299 **4. Implications**

300 Several studies (Blewett et al., 2013; Helbert et al., 2013a) suggested that the  
301 formation of hollows can be attributed to the thermal decomposition/sublimation of  
302 volatile-rich minerals such as sulfides constituting the hollow materials. (Thomas et al.,  
303 2014a) conducted a global investigation of hollows on Mercury for its extent and size  
304 in order to understand their formation mechanism. The study showed that the hollows  
305 in the northern hemisphere are preferentially on sun-facing slopes implying a formation  
306 mechanism related to solar heating.

307 The emissivity of sulfides (7-14  $\mu\text{m}$ ) as a function of temperature under  
308 simulated Mercury daytime surface conditions showed that most of the proposed  
309 sulfides (MgS, FeS, CrS, TiS, NaS, and MnS) show spectrally evolving emissivity  
310 behavior changes with increasing surface temperatures (Varatharajan et al., 2019). This  
311 further suggests that these sulfides thermally decompose and sublime when exposed  
312 to extreme thermal environment of Mercury, and probably form hollows.

313 Previous studies show that Mercury's 2:3 orbital resonance has a significant  
314 impact on the latitudinal and longitudinal dependence on the peak surface temperatures  
315 during Mercury days (Bauch et al., 2021; Krotikov and Shchuko, 1975; Soter and  
316 Ulrichs, 1967; Vasavada et al., 1999). Therefore, it is important to understand the  
317 maximum daytime temperature distribution of Mercury along with the spatial  
318 distribution of hollows for their effective mapping and detection (Helbert et al., 2013a;  
319 Vilas et al., 2016). In order to achieve this, we re-created the modeled temperature map

320 of Mercury derived from Bauch et al. (2021) which was mapped for Mercury latitudes  
 321 between 60 °N and 60 °S and we overlaid the globally mapped hollow groups of  
 322 Thomas et al. (2014a) (Fig. 5). The locations of hollow groups are re-mapped from the  
 323 supplementary file provided in Thomas et al. (2014a). Both surface temperature and  
 324 hollow distribution are overlaid on the MESSENGER MDIS Map Projected Low-  
 325 Incidence Angle Basemap (LOI) of global monochrome map (750 nm) at a resolution  
 326 of 256 pixels per degree (~166 m/pix) (Denevi et al., 2018; Hawkins et al., 2007) (Fig.  
 327 5).  
 328



329  
 330  
 331  
 332  
 333  
 334  
 335  
 336  
 337  
 338  
 339  
 340

**Figure 5.** The peak surface temperature distribution across Mercury surface is mapped from (Bauch et al., 2021). The surface temperatures are overlaid on the MESSENGER MDIS global Map Projected Low-Incidence Angle Basemap (LOI) data set consists of a global monochrome map (750 nm) of reflectance at a resolution of 256 pixels per degree (~166 m/pix) (Denevi et al., 2018; Hawkins et al., 2007). The black datapoints indicate the distribution of hollows across Mercury’s surface mapped by Thomas et al. (2014). The hollows within the Tyagaraja (3.89°N, 328.9°E), Dominici (1.38°N, 323.5°E), and Hopper (12.4°S 304.1°E) craters and NE Rachmaninoff (27.6°N, 57.4°E) are marked by white crosses.

341 Fig. 5 shows that hollows are distributed globally irrespective of the varying  
342 peak surface temperatures ( $T_{\text{peak}}$ ). The total number of hollows in regions between 60  
343 °N and 60 °S with peak daytime surface temperatures above ~300 °C (orange to red;  
344 Fig. 5) and below ~300 °C (blue to yellow; Fig. 5) are 275 and 151 respectively. Some  
345 notable examples are volcanic materials within the NE Rachmaninoff basin (27.6 °N,  
346 57.4 °E) which are located within the temperature regime  $\sim 277\text{ °C} < T_{\text{peak}} < \sim 308\text{ °C}$   
347 (light green) whereas hollows within the Tyagaraja (3.89 °N, 328.9 °E) and Dominici  
348 (1.38 °N, 323.5 °E) craters are located in areas within  $\sim 369\text{ °C} < T_{\text{peak}} < \sim 399\text{ °C}$   
349 (intermediate red). Hopper (12.4 °S, 304.1 °E) crater is located within the temperature  
350 regime  $\sim 308\text{ °C} < T_{\text{peak}} < \sim 338\text{ °C}$  (yellow) in Fig. 5. This compels the need for study for  
351 creating unique spectral library of various hollow-forming materials such as sulfides as  
352 a function of varying surface temperatures of Mercury (Varatharajan et al., 2019).

353 CaS belongs to the group of proposed sulfides of Mercury that constitute the  
354 chemical composition of surface features of presumably volcanic origin – such as  
355 hollow-forming minerals and pyroclastics (Besse et al., 2020; Helbert et al., 2013a;  
356 Vilas et al., 2016). In volcanic terrains, CaS has been proposed and spectrally detected  
357 in the hollows in visible-infrared spectral region using the MDIS data (Helbert et al.,  
358 2013a; Vilas et al., 2016). Varatharajan et al. (2019) demonstrated that most sulfides  
359 (MgS, FeS, CrS, TiS, NaS, and MnS) except for CaS are both physically and spectrally  
360 unstable when exposed to extreme daytime thermal environment of Mercury. The  
361 results from our study where CaS is exposed to repeated heating cycles under simulated  
362 Mercury daytime surface conditions (up to 500 °C), strongly suggest that CaS is the  
363 most stable sulfide against thermal weathering on Mercury's surface. This indirectly  
364 suggests that unlike other sulfides (MgS, FeS, CrS, TiS, NaS, and MnS), CaS may not  
365 significantly contribute to hollow formation on Mercury by solar heating as CaS does

366 not decompose with repeated heating cycles even under extreme temperatures reaching  
367 up to 500 °C. This would make CaS (if detected and mapped by MERTIS) a good tracer  
368 for sulfides (possibly among other volatiles) on Mercury that leads to formation of  
369 hollows, as other sulfides are lost in sublimation leaving behind the hollows.

370 In fact, CaS was successfully detected within the hollows of Dominici and  
371 Hopper craters (Vilas et al., 2016) and these craters occur in surface regions where peak  
372 temperatures reach ~400 °C as marked in Fig. 5. Future studies that combine the global  
373 mapping of CaS, the extent and depth of hollows bearing CaS and other sulfides will  
374 give further insight into the nature of volatiles on Mercury's surface and its interior as  
375 well as hollow forming mechanisms. As the emissivity behavior of pure CaS does not  
376 evolve with increasing surface temperatures, CaS can be globally mapped irrespective  
377 of the peak surface temperatures/heating cycles across Mercury.

378 Furthermore, the spectral investigation of various sulfides by Varatharajan et al.  
379 (2019) showed that the TIR spectral region is sensitive for the detection and  
380 characterization of sulfide minerals under Mercury daytime conditions. Hence,  
381 MERTIS onboard the BepiColombo mission will support the global mapping of  
382 volatiles on Mercury's surface and will help understanding the hollow forming  
383 mechanisms and its materials. Ultimately, such studies will help calculating the volatile  
384 budget of Mercury's interior and its contributions to Mercury's exosphere.

385

## 386 **5. Conclusions**

387 In this study, the physical and spectral stability of CaS has been investigated for  
388 four simulated Mercury days (heating cycles). The study indicates that calcium sulfide  
389 (CaS) is stable on Mercury's surface with emissivity spectra retaining their  
390 characteristic features irrespective of surface temperatures and repeated heating cycles

391 typical for Mercury. At all surface temperatures, the presence of CaS on Mercury  
392 surface can be identified by its emissivity behavior in the TIR spectral region (7-14  $\mu\text{m}$ )  
393 which is characterized by a) a spectral minimum at  $\sim 7.5 \mu\text{m}$  and  $9.5 \mu\text{m}$ , b) an  
394 emissivity maximum centered around  $\sim 8.8 \mu\text{m}$  with a peak doublet, and c) a broad  
395 spectral band between 10 and 12  $\mu\text{m}$ . Our study demonstrates that CaS is the least  
396 thermally weathered sulfide among those expected on Mercury's surface, making it a  
397 good tracer for the presence of sulfides (possibly among other volatiles) associated with  
398 hollows and pyroclastics when globally mapped by MERTIS. The unique spectral  
399 library provided with this work will support global mapping of CaS around hollows and  
400 pyroclastic materials of Mercury surface using MERTIS payload onboard  
401 BepiColombo mission. The global mapping of CaS along with other sulfides across  
402 hollows will further help our understanding of the hollow formation mechanism  
403 dominated by sublimation process.

404

#### 405 **Acknowledgements**

406 IV thank DLR/DAAD Doctorate Fellowship for funding her PhD work at PSL-  
407 DLR. A portion of this research was supported by the European Union's Horizon 2020  
408 research and innovation program. Europlanet 2020 RI has received funding from the  
409 European Union's Horizon 2020 research and innovation programme under grant  
410 agreement No 654208.

411

#### 412 **References**

413 Bauch, K.E., Hiesinger, H., Greenhagen, B.T., Helbert, J., 2021. Estimation of surface  
414 temperatures on Mercury in preparation of the MERTIS experiment onboard  
415 BepiColombo. *Icarus* 354, 114083.

416 Besse, S., Doressoundiram, A., Barraud, O., Griton, L., Cornet, T., Muñoz, C.,  
417 Varatharajan, I., Helbert, J., 2020. Spectral Properties and Physical Extent of  
418 Pyroclastic Deposits on Mercury: Variability Within Selected Deposits and  
419 Implications for Explosive Volcanism. *Journal of Geophysical Research:*  
420 *Planets* 125, e2018JE005879.

421 Blewett, D.T., Vaughan, W.M., Xiao, Z., Chabot, N.L., Denevi, B.W., Ernst, C.M.,  
422 Helbert, J., D'Amore, M., Maturilli, A., Head, J.W., Solomon, S.C., 2013.  
423 Mercury's hollows: Constraints on formation and composition from analysis of  
424 geological setting and spectral reflectance. *Journal of Geophysical Research:*  
425 *Planets* 118, 1013-1032.

426 Denevi, B.W., Chabot, N.L., Murchie, S.L., Becker, K.J., Blewett, D.T., Domingue,  
427 D.L., Ernst, C.M., Hash, C.D., Hawkins, S.E., III, Keller, M.R., Laslo, N.R.,  
428 Nair, H., Robinson, M.S., Seelos, F.P., Stephens, G.K., Turner, F.S., Solomon,  
429 S.C., 2018. Calibration, Projection, and Final Image Products of  
430 MESSENGER's Mercury Dual Imaging System. *Space Science Reviews* 214.

431 Hawkins, S.E., Boldt, J.D., Darlington, E.H., Espiritu, R., Gold, R.E., Gotwols, B.,  
432 Grey, M.P., Hash, C.D., Hayes, J.R., Jaskulek, S.E., 2007. The Mercury dual  
433 imaging system on the MESSENGER spacecraft. *Space Science Reviews* 131,  
434 247-338.

435 Helbert, J., Dyar, D., Maturilli, A., Widemann, T., Marcq, E., Rosas-Ortiz, Y., Walter,  
436 i., D'Amore, M., Alemanno, G., Mueller, N., Smrekar, S., 2019. Spectroscopy

437 of the Surface of Venus - in the Laboratory and from Orbit, EPSC-DPS Joint  
438 Meeting 2019.

439 Helbert, J., Maturilli, A., 2009. The emissivity of a fine-grained labradorite sample at  
440 typical Mercury dayside temperatures. *Earth and Planetary Science Letters* 285,  
441 347-354.

442 Helbert, J., Maturilli, A., D'Amore, M., 2013a. Visible and near-infrared reflectance  
443 spectra of thermally processed synthetic sulfides as a potential analog for the  
444 hollow forming materials on Mercury. *Earth and Planetary Science Letters* 369–  
445 370, 233-238.

446 Helbert, J., Nestola, F., Ferrari, S., Maturilli, A., Massironi, M., Redhammer, G.J.,  
447 Capria, M.T., Carli, C., Capaccioni, F., Bruno, M., 2013b. Olivine thermal  
448 emissivity under extreme temperature ranges: Implication for Mercury surface.  
449 *Earth and Planetary Science Letters* 371–372, 252-257.

450 Hiesinger, H., Helbert, J., Alemanno, G., Bauch, K.E., D'Amore, M., Maturilli, A.,  
451 Morlok, A., Reitze, M.P., Stangarone, C., Stojic, A.N., Varatharajan, I., Weber,  
452 I., the, M.C.-I.T., 2020. Studying the Composition and Mineralogy of the  
453 Hermean Surface with the Mercury Radiometer and Thermal Infrared  
454 Spectrometer (MERTIS) for the BepiColombo Mission: An Update. *Space*  
455 *Science Reviews* 216, 110.

456 Hiesinger, H., Helbert, J., MERTIS Co-I Team, 2010. The Mercury Radiometer and  
457 Thermal Infrared Spectrometer (MERTIS) for the BepiColombo mission.  
458 Planetary and Space Science 58, 144-165.

459 Krotikov, V., Shchuko, O., 1975. Thermal conditions in the surface layer of Mercury.  
460 Soviet Astronomy 19, 86-89.

461 Lucchetti, A., Pajola, M., Galluzzi, V., Giacomini, L., Carli, C., Cremonese, G., Marzo,  
462 G.A., Ferrari, S., Massironi, M., Palumbo, P., 2018. Mercury Hollows as  
463 Remnants of Original Bedrock Materials and Devolatilization Processes: A  
464 Spectral Clustering and Geomorphological Analysis. Journal of Geophysical  
465 Research: Planets 123, 2365-2379.

466 Maturilli, A., Donaldson Hanna, K.L., Helbert, J.r., Pieters, C., 2013. A New Standard  
467 for Calibration of High Temperature Emissivity: Laboratory Intercalibration at  
468 PEL of DLR and ALEC of Brown University, LPSC 2013.

469 Maturilli, A., Helbert, J., Moroz, L., 2008. The Berlin emissivity database (BED).  
470 Planetary and Space Science 56, 420-425.

471 Nittler, L.R., Starr, R.D., Weider, S.Z., McCoy, T.J., Boynton, W.V., Ebel, D.S., Ernst,  
472 C.M., Evans, L.G., Goldsten, J.O., Hamara, D.K., Lawrence, D.J., McNutt,  
473 R.L., Schlemm, C.E., Solomon, S.C., Sprague, A.L., 2011. The Major-Element  
474 Composition of Mercury's Surface from MESSENGER X-ray Spectrometry.  
475 Science 333, 1847-1850.

476 Soter, S., Ulrichs, J., 1967. Rotation and Heating of the Planet Mercury. *Nature* 214,  
477 1315-1316.

478 Thomas, R.J., Rothery, D.A., Conway, S.J., Anand, M., 2014a. Hollows on Mercury:  
479 Materials and mechanisms involved in their formation. *Icarus* 229, 221-235.

480 Thomas, R.J., Rothery, D.A., Conway, S.J., Anand, M., 2014b. Long-lived explosive  
481 volcanism on Mercury. *Geophysical Research Letters* 41, 6084-6092.

482 Varatharajan, I., Maturilli, A., Helbert, J., Alemanno, G., Hiesinger, H., 2019. Spectral  
483 behavior of sulfides in simulated daytime surface conditions of Mercury:  
484 Supporting past (MESSENGER) and future missions (BepiColombo). *Earth  
485 and Planetary Science Letters* 520, 127-140.

486 Vasavada, A.R., Paige, D.A., Wood, S.E., 1999. Near-Surface Temperatures on  
487 Mercury and the Moon and the Stability of Polar Ice Deposits. *Icarus* 141, 179-  
488 193.

489 Vaughan, W.M.H., J. W.; Parman, S. W.; Helbert, J. , 2013. What Sulfides Exist on  
490 Mercury? 44th Lunar and Planetary Science Conference 2013.

491 Vilas, F., Domingue, D.L., Helbert, J., D'Amore, M., Maturilli, A., Klima, R.L.,  
492 Stockstill-Cahill, K.R., Murchie, S.L., Izenberg, N.R., Blewett, D.T., Vaughan,  
493 W.M., Head, J.W., 2016. Mineralogical indicators of Mercury's hollows  
494 composition in MESSENGER color observations. *Geophysical Research  
495 Letters* 43, 1450-1456.

496 Weider, S.Z., Nittler, L.R., Murchie, S.L., Peplowski, P.N., McCoy, T.J., Kerber, L.,  
497 Klimczak, C., Ernst, C.M., Goudge, T.A., Starr, R.D., Izenberg, N.R., Klima,  
498 R.L., Solomon, S.C., 2016. Evidence from MESSENGER for sulfur- and  
499 carbon-driven explosive volcanism on Mercury. *Geophysical Research Letters*  
500 43, 3653-3661.

501 Weider, S.Z., Nittler, L.R., Starr, R.D., McCoy, T.J., Solomon, S.C., 2014. Variations  
502 in the abundance of iron on Mercury's surface from MESSENGER X-Ray  
503 Spectrometer observations. *Icarus* 235, 170-186.

504 Weider, S.Z., Nittler, L.R., Starr, R.D., McCoy, T.J., Stockstill-Cahill, K.R., Byrne,  
505 P.K., Denevi, B.W., Head, J.W., Solomon, S.C., 2012. Chemical heterogeneity  
506 on Mercury's surface revealed by the MESSENGER X-Ray Spectrometer.  
507 *Journal of Geophysical Research: Planets* 117, n/a-n/a.  
508